

Electronic states in mixed pseudobinary (Pb,Sr)S crystals

J. Kudrnovský* and N. E. Christensen†

Max-Planck-Institut für Festkörperforschung, Heisenbergstrasse 1, 7000 Stuttgart 80, Germany

(Received 13 December 1990)

The energy bands of lead and strontium sulfides in the rock-salt structure are determined using the scalar-relativistic linear-muffin-tin-orbitals method. The effect of spin-orbit coupling is discussed for the case of PbS. The results are subsequently used for the study of concentration trends in the densities of states and the Bloch spectral densities for (Pb,Sr)S mixed crystals within the coherent-potential approximation. Comparison is made with a previous study based on the empirical tight-binding model.

I. INTRODUCTION

Mixed semiconductors are substitutional solutions of semiconducting compounds. These materials have attracted much interest because of their ability to produce device materials with customized properties. Typical examples are isoelectronic pseudobinary alloys $A_xB_{1-x}C$, in which the atoms A and B belong to the same group of the Periodic Table and thus have the same number of valence electrons as well as, crudely speaking, the same valency. Sometimes, as in III-V (or II-VI) mixed crystals, the electronic structure smoothly interpolates between the constituent crystals $A^{\text{III}}C^{\text{V}}$ and $B^{\text{III}}C^{\text{V}}$ (or $A^{\text{II}}C^{\text{VI}}$ and $B^{\text{II}}C^{\text{VI}}$) and the simple virtual-crystal approximation (VCA) becomes justified. The characteristic example is the (Ga,Al)As alloy. In some cases the quantitative difference between the constituents is so large that the VCA breaks down and more sophisticated methods, such as the coherent-potential approximation¹⁻³ (CPA) or the recursion⁴ or the supercell⁵ methods, must be used. This has been demonstrated in a study of the deep-lying valence states in (Cd,Hg)Te mixed crystals.^{2,3} Recently, a new class of semiconducting mixed crystals has been prepared by combining II-VI semiconductors with IV-VI compounds over a wide concentration range as, for instance, in the (Pb,Sr)S system.⁶ In addition to practical device applications in the device physics, these mixed systems are also interesting from the theoretical point of view. The substitution in $A_x^{\text{II}}B_{1-x}^{\text{IV}}C^{\text{VI}}$ mixed crystals is not isoelectronic but only isovalent because of the different configurations of their valence shells. Thus Sr has a $5s^2$ outer shell while that of Pb is $6s^26p^2$. Note that the Pb $6s^2$ electrons form an inert pair while Pb $6p^2$ electrons are involved in the bonding similarly to the outer s^2 electrons of the group IIa metals ($5s^2$ in Sr). However, the role of "inert" Pb $6s^2$ electrons is crucial to a proper description of the electronic structure because they strongly mix with the S $3p$ states.⁴ The Sr and Pb potentials differ so much that the electronic structure of (Pb,Sr)S mixed crystals will be strongly affected by alloying, and the use of the VCA is meaningless. The electronic properties of the (Pb,Sr)S system have recently been studied theoretically.^{4,7} The calculations were based

on the empirical tight-binding (TB) Hamiltonian with parameters fitted⁴ empirically to available *ab initio* band-structure calculations for pure PbS and SrS, which both crystallize in the rock-salt structure. The alloy effects were treated properly by using the recursion method applied to a large cluster of atoms. The principal drawback of empirical schemes, especially when alloys are concerned, is an uncertainty in the determination of the Hamiltonian parameters, even if the same fitting procedure is used for both constituent crystals. This is especially serious when the constituent band structures are very different. The energies in the high-symmetry points in the Brillouin zone can usually be well reproduced, but the band curvatures between these are often poorly accounted for, especially for the conduction states. Although the results are sometimes satisfactory, the need for an alloy theory based on first principles, rather than on empirical descriptions is clear. Such a theory, based on the linear-muffin-tin-orbitals method within the atomic-sphere approximation (LMTO-ASA) and the CPA, has been developed by us recently,^{3,8} and applied to semiconductor mixed crystals with the zinc-blende structure.³ The main purpose of this paper is to apply it to mixed (Pb,Sr)S crystals with the rock-salt structure. We determine the local densities of states and the Bloch spectral densities as functions of the alloy composition, and compare the results with the empirical TB calculation of Ref. 4.

II. CALCULATION METHOD

Our starting point is the Hamiltonian of the pseudobinary $\text{Pb}_x\text{Sr}_{1-x}\text{S}$ mixed crystal with the rock-salt structure and in the orthogonal LMTO representation:⁹

$$H_{RL,R'L'} = C_{RL} \delta_{RR'} \delta_{LL'} + \Delta_{RL}^{1/2} [S^0(1 - \gamma S^0)^{-1}]_{RL,R'L'} \Delta_{R'L'}^{1/2}. \quad (1)$$

Here, R labels the site, and $L = (l, m)$ is the collective orbital-angular-momentum index. For a good space filling, the interstitial empty spheres were introduced into the rock-salt structure. Equal sphere sizes were assumed

on all sites in order to minimize the overlap. The sites define the underlying lattice which is bcc with halved lattice constant, characterized by the nonrandom structure matrix S^0 . The rock-salt structure is described as an interpenetration of four fcc sublattices displaced along the bcc body diagonal by $(\frac{1}{4}, \frac{1}{4}, \frac{1}{4})a$, where a is the lattice constant. The first sublattice is occupied randomly by Pb and Sr cations, the second and fourth sublattices are occupied by (identical) empty spheres, and the third one by sulfur atoms. The potential parameters X_{RL} entering the expansion for the Hamiltonian characterize the scattering properties of atoms on sublattices. The scalar-relativistic LMTO-ASA band-structure method¹⁰ in conjunction with the local-density approximation (LDA) using the von Barth–Hedin exchange and correlation potential was used to generate self-consistently the potential parameters for PbS and SrS at their experimental equilibrium volumes. The spin-orbit coupling term was then added perturbatively to the Hamiltonian to estimate its effects for PbS. The potential parameters of PbS and SrS were used to generate a model of (Pb,Sr)S mixed crystals as follows. (i) On cation sites we use either PbS or SrS potential parameters, depending on whether the sites were occupied by Pb or Sr. (ii) On anion sites (as well as on the empty spheres) we average PbS and SrS potential parameters corresponding to these sites. One can average them, for example, according to the number of neighboring Pb and Sr atoms to the S atom. Another possibility, employed here, is to include these differences also within the CPA. Concerning the configurational averaging, we note that our TB-LMTO method takes into account both the diagonal and off-diagonal randomness on equal footing.⁸ The potential parameters of PbS and SrS were determined from the LMTO method with the sp^3d^5 partial waves on all atomic and empty sphere sites, which leads to a 36×36 problem. A minimal basis set suffices for an accurate description of the valence and low-lying conduction states, provided that remaining states are not neglected, but included approximately by means of Löwdin down folding. The linearization of the contribution of the down-folded states is performed in a suitably chosen LMTO representation around the energy ε_0 , which is at the center of the energy range of interest. Alternatively, one can use more energy panels centered at ε_{01} , ε_{02} , etc. for a broader energy range of interest. As a result, the solution to the problem is obtained within a minimal basis set alone, which is convenient from computational as well as interpretational points of view.

III. RESULTS AND DISCUSSION

The band structures of PbS and SrS, determined by the diagonalization of the Hamiltonian (1) in the full basis, are given in Figs. 1 and 2, respectively. The minimal basis set $\text{Pb}(\text{Sr})(sp^3d^5)E(s)S(p^3)E(s)$, where $\text{Pb}(\text{Sr})$ stands for the cations and E for the empty spheres, gives an excellent description of the valence and low-lying conduction states (14×14 model). We use two energy panels: The valence Pb s states between -0.85 and -0.5 Ry are described with the energy of linearization $\varepsilon_0 = -0.7$ Ry, while remaining valence and low-lying

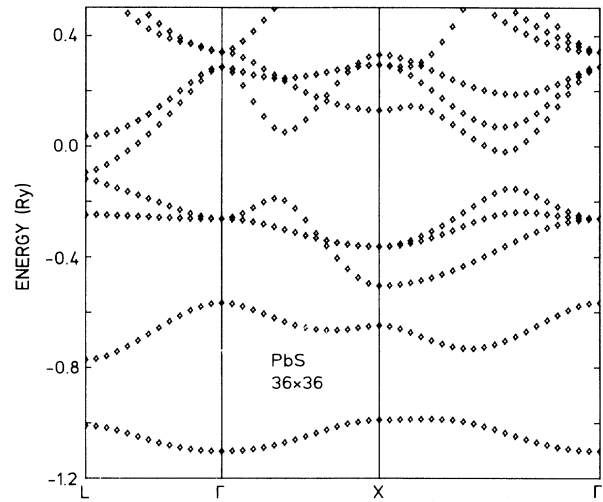


FIG. 1. The scalar-relativistic bands of PbS along the lines $L-\Gamma-X-\Gamma$ in the fcc Brillouin zone. The full LMTO basis is employed.

conduction states in the energy range -0.55 to 0.4 Ry employ $\varepsilon_0 = -0.1$ Ry. The two energy panels are separated by a gap. A one-panel calculation with $\varepsilon_0 = -0.2$ Ry gives nearly the same results for the valence and low-lying conduction states, but the position of the deep-lying Pb s states at the X point is slightly shifted from the value found in the full 36×36 model. The two-panel down-folding scheme reproduces the full bands correctly, and this will therefore be used throughout. We note that the deep-lying valence S s states are outside the energy range of interest; otherwise they should also be included in the minimal basis set. Even smaller minimal basis sets can be used in particular cases. For example, the 9×9 model $\text{Pb}(sp^3)E(s)S(p^3)E(s)$ gives an equally good description

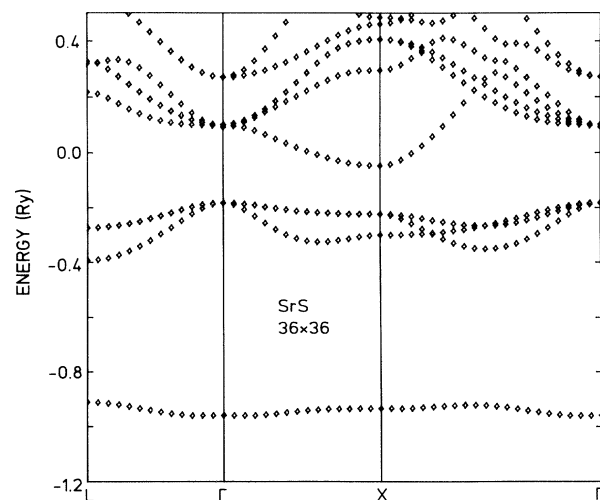


FIG. 2. As in Fig. 1, but for SrS.

as the 14×14 model in the energy range studied. On the other hand, the Sr d states are essential for a proper description of the first few conduction bands. We note that for the application to random alloys, the minimal basis must be common for both end-point crystals³ PbS and SrS, which results in the use of the 14×14 model described above. The band structure of PbS with the spin-orbit coupling included, and for the 9×9 model (18×18 model with the spin-orbit term) is shown in a reduced energy range in Fig. 3. The following values of the spin-orbit parameters ξ_p were employed: $\xi_p^{\text{Pb}} = 0.12$ Ry, and $\xi_p^{\text{S}} = 0.005$ Ry. There is overall good agreement for PbS between the empirical-pseudopotential-method calculations of Ref. 11, and our self-consistent calculations, Figs. 1 and 3, in the corresponding energy ranges. The orbital decomposition of the states is as follows. The Pb p states contribute to the conduction bands. The upper part of the valence states for energies between -0.5 and -0.1 Ry has mainly the anion p character, while two deep-lying valence states are due to the Pb s and S s states. The simple scheme is modified by the hybridization. There is an important coupling between the anion and cation p states. The anion p states hybridize also with the cation s states. The influence of the spin-orbit coupling is much stronger for the conduction bands because they originate, as already mentioned, from the Pb p states with non-negligible spin-orbit coupling constant ξ_p^{Pb} . Despite the fact that the spin-orbit effects introduce some qualitative changes, especially the lowering of the degeneracy of some bands, the scalar-relativistic description is satisfactory for our purposes, and it also simplifies the CPA calculations. The spin-orbit effects were also neglected in Ref. 4.

The SrS bands compare reasonably well with the non-relativistic self-consistent augmented-plane-wave (APW) calculations with Slater exchange of Ref. 12. The most pronounced difference is the valence-band width: 0.21

Ry in our case as compared with 0.16 Ry in Ref. 12. The insulating gap in SrS is underestimated as is usual in the LDA. This can be remedied empirically within the LMTO-ASA method.¹³ However, due to the limited experimental information available, no attempt was made here to adjust the LDA gap. The deep-lying narrow S s states are well separated from the valence states which are essentially of the S p character. The minimum of the conduction bands lies at the X point, so that the gap in SrS is indirect. The lowest conduction bands consist mostly of Sr d states. We note that the d states at the X point almost have lost their atomic $4d$ character, and thus have rather a plane-wave-like character.¹² The Γ conduction state is mainly Sr s -like. The influence of the spin-orbit coupling for the SrS crystal is less important¹⁴ than for the PbS.

The alloys studied exhibit the so-called split-band-limit behavior for the cation s , p , and d states, which invalidates simplified treatments like the VCA. To be specific, the values of the band-center potential parameter C give us a feeling of the strength of the level disorder: $C_s^{\text{Pb}} = 1.02$ Ry, $C_s^{\text{Sr}} = 0.76$ Ry; $C_p^{\text{Pb}} = 0.20$ Ry, $C_p^{\text{Sr}} = -1.58$ Ry; and $C_d^{\text{Pb}} = 2.29$ Ry, $C_d^{\text{Sr}} = 0.59$ Ry. Systems with such a strong level disorder can be treated by the CPA method. Alternatively, one can use either the recursion⁴ or the supercell⁵ approaches which are also able to treat correctly the strong-scattering limit case present in the (Pb,Sr)S mixed crystals. There is also non-negligible off-diagonal disorder in the nearest-neighbor Pb-S and Sr-S hopping integrals. We note that our method takes these differences into account on the same level of accuracy as the diagonal disorder,⁸ similarly to the Korringa-Kohn-Rostoker coherent-potential approximation (KKR-CPA) approach.

The concentration trends of the total density of states (DOS) for (Pb,Sr)S mixed crystals are shown in Fig. 4 for the 14×14 model and for the results in two energy panels assembled together. The most remarkable feature of alloying when Pb atoms are added into the SrS crystal is the development of the Pb-related DOS peak centered around $E \approx -0.7$ Ry. The weight of this peak and its width increases with the Pb content. The deep-lying common alloy S s band is outside the energy window shown in the figure. Another effect is the shape development and broadening, with increasing Pb concentration, of the main valence band dominated by the S p states. The total number of states in this band remains unchanged. This broadening is due to varying nearest-neighbor environment with the alloy composition, primarily the greater hybridizational hopping integral between Pb p and S p states as compared with Sr p and S p states. Note also the increase of the gap with increasing Sr concentration. The lowest conduction bands exhibit a strong shape development due to different orbital composition of these states in PbS (Pb p states) and SrS (Sr d states). Finally, we note small, but non-negligible contribution of the down-folded states into the total DOS (dotted lines in Fig. 4).

The orbital decomposition of the total DOS (its minimal-basis-set contribution) for the $\text{Pb}_{0.5}\text{Sr}_{0.5}\text{S}$ mixed crystal is presented in Fig. 5 for the largest components.

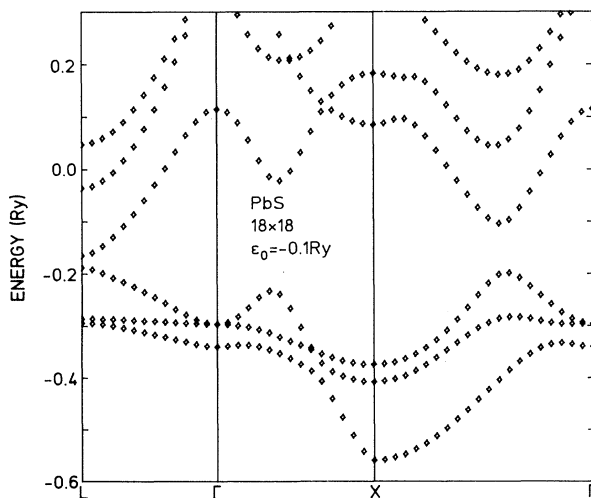


FIG. 3. The relativistic energy bands of PbS along $L-\Gamma-X-\Gamma$. The minimal basis set consists of $\text{Pb}(sp^3)E(s)\text{S}(p^3)E(s)$; the remaining states are included approximately via Löwdin down folding (18×18 model, $\epsilon_0 = -0.1$ Ry).

The Pb *s* states dominate the lowest valence band, but they also contribute to the upper part of the alloy valence bands. The valence states are primarily S *p*-like. The lowest conduction bands are dominated by the Pb *p* and Sr *d* states. The Pb *p* states also contribute to the lower part of the alloy valence band. Qualitatively similar results were obtained by the empirical tight-binding recursion method of Davis,⁴ but quantitative differences are found. These are due primarily to the approximate description of the lowest conduction states within the empirical TB Hamiltonian as well as to the sensitivity of the recursion method to the boundary conditions (number of recursions, size and shape of the cluster, etc.).

The Bloch spectral densities for three alloy compositions corresponding to the alloy compositions of Fig. 6 are plotted in Fig. 6 along the line $L-\Gamma-X$ in the fcc Brillouin zone. The Bloch spectral density is defined in terms of the configurationally averaged resolvent $\langle G(z) \rangle$ corresponding to the alloy Hamiltonian (1) in the following manner:

$$A(k, E) = -\frac{1}{\pi} \text{Im} \sum_L \langle kL | \langle G(E + i0) \rangle | kL \rangle. \quad (2)$$

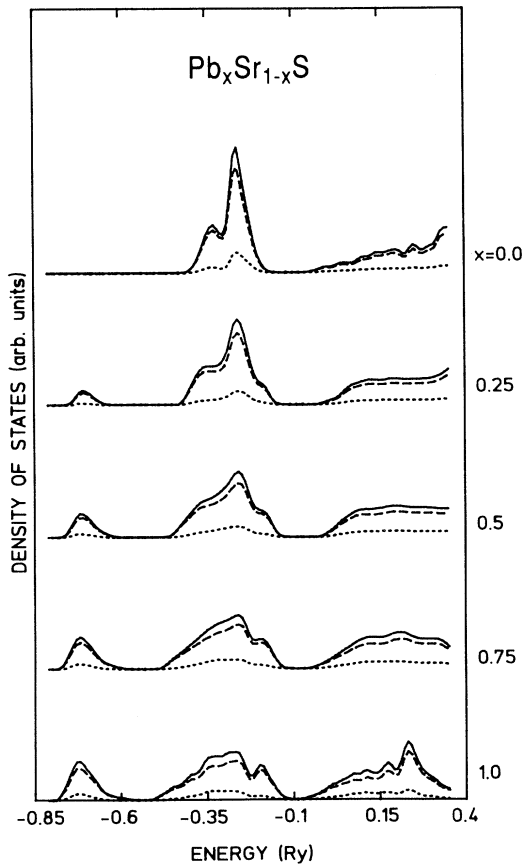


FIG. 4. The total densities of states for $\text{Pb}_x\text{Sr}_{1-x}\text{S}$ mixed crystals (solid lines) and their decomposition into the contributions from the minimal basis set (dashed lines) and from remaining states (dotted lines). The concentrations are assigned to the corresponding curves (14×14 model, $\epsilon_0 = -0.7$ and -0.1 Ry).

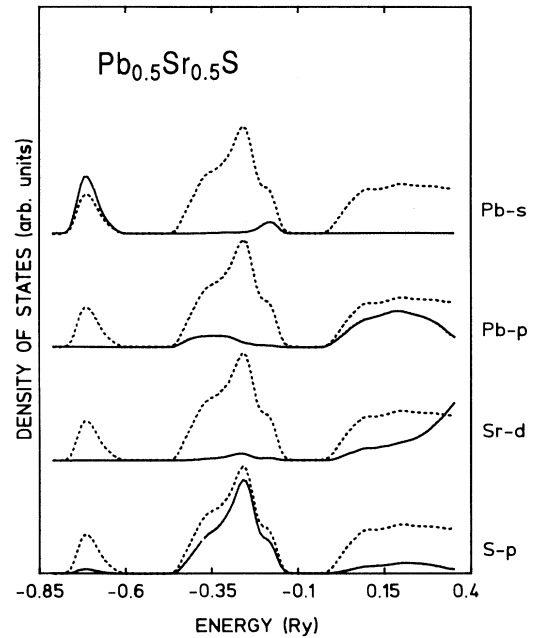


FIG. 5. The decomposition of the minimal-basis-set part of the total density of states (dotted) for $\text{Pb}_{0.5}\text{Sr}_{0.5}\text{S}$ mixed crystal into the dominating atom- and orbital-resolved contributions (14×14 models, $\epsilon = -0.7$ and -0.1 Ry).

In the crystal, the spectral densities are δ functions centered at the energies of corresponding bands. In random alloys they are shifted and broadened by the disorder. For a weak scattering they have a form of Lorentzian-like peaks centered at the VCA energies. It is thus instructive to consult the band structures of pure PbS and SrS, Figs.

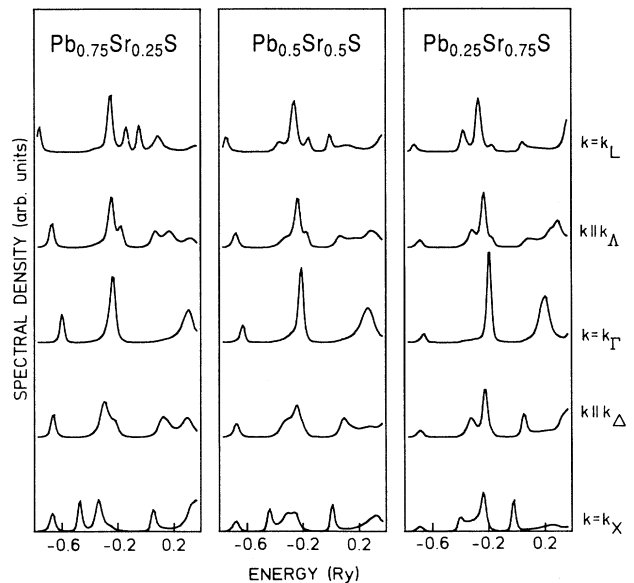


FIG. 6. The Bloch spectral densities along $L-\Gamma-X$ in the fcc Brillouin zone for $\text{Pb}_{0.75}\text{Sr}_{0.25}\text{S}$ (left panel), $\text{Pb}_{0.5}\text{Sr}_{0.5}\text{S}$ (middle panel), and $\text{Pb}_{0.25}\text{Sr}_{0.75}\text{S}$ (right panel) mixed crystals.

1 and 2, in the foregoing discussion. The spectral densities are evaluated assuming a constant broadening of 0.005 Ry. The lowest, strongly \mathbf{k} -dispersive peak in the Pb-rich alloy corresponds to the Pb_s -derived states. These states are more broadened and less dispersive in the Sr-rich alloy, where they represent the impurity states. The valence states at the Γ point are only weakly influenced by disorder (a sharp narrow peak at $E \approx -0.2$ Ry). This should be contrasted with the conduction-band peak at the Γ point, which is much more broadened by disorder and shifted downward with increasing Sr concentration. Let us discuss the concentration trends at the X point. We first note the increase of the direct band gap with the increasing Pb content. A similar result was obtained in Ref. 4. The dominating peak at $E \approx -0.25$ Ry for the Sr-rich alloy is strongly suppressed upon addition of Pb atoms, and in the Pb-rich alloy it survives only as a shoulder indicating the strong influence of the alloy disorder in this energy region. On the contrary, the peaks at $E \approx -0.5$ and -0.35 Ry in the Pb-rich case, which are the remnants of the corresponding bands in pure PbS, are shifted and have lost their intensity when the Sr atoms are added. At the L point, and for the Sr-rich alloy, the two dominating peaks are remnants of the SrS bands. The second peak at $E \approx -0.4$ Ry survives in the Pb-rich alloy again only as a shoulder. The three small peaks at $E \approx -0.75$, -0.15 , and 0.0 Ry are remnants of the PbS bands, and they increase in intensity with increasing Pb concentration.

Two remarks are now in order. Firstly, the strong broadening of some bands in certain energy regions indicates that the well-known selection rules for the vertical optical transitions in crystals could be relaxed in random alloys, thus making nonvertical optical transitions mediated by the disorder possible. Secondly, at the high-symmetry points in the Brillouin zone, it is possible to divide the spectral density into the contributions of a

given symmetry. For example, at the X point it is possible to split the spectral density into parts corresponding to the X_3 and X'_5 contributions. Only the total spectral density, which is the trace over all symmetries [see Eq. (2)], is presented in this paper as we wish to calculate the spectral densities also for \mathbf{k} points with lower symmetry, e.g., along the line $\Gamma-X$. Keeping this fact in mind, the results of Ref. 4 agree reasonably well¹⁵ with ours. Finally, we note that the detailed discussion of the lowest conduction bands, especially of their \mathbf{k} -dependent properties reflected in the Bloch spectral densities, requires the inclusion of the spin-orbit-coupling effects (compare Figs. 1 and 3).

In conclusion, we have applied the first-principles TB-LMTO-CPA method to evaluate the electronic properties of disordered semiconductor alloys which crystallize in the rock-salt structure. For the specific cases of (Pb,Sr)S mixed crystals, our results support the main qualitative conclusions made on the basis of the empirical method of Ref. 4. The recursion method treats correctly strong electron scattering in random alloys, but its success depends sensitively on the choice of the empirical parameters for the alloy Hamiltonian, i.e., on the choice of the values of atomic levels and hopping integrals. Also, the values of the mixed hopping integrals between Pb and Sr atoms must be guessed in some way.¹⁶ These problems do not occur in our theory, where the structural and scattering properties are separated into the structure constants and potential parameters, respectively. The potential parameters are determined from first principles within the LDA framework. Finally, although the recursion method is also able to give information about the \mathbf{k} -dependent properties (the Bloch spectral density is just the simplest property of that type), these results are more sensitive to the cluster size and boundary conditions than the local quantities, such as the total and component densities of states.

*Permanent address: Institute of Physics, Czechoslovak Academy of Sciences, Na Slovance 2, 180 40 Praha, Czechoslovakia.

†Present address: Institute of Physics, University of Aarhus, DK-8000 Aarhus C, Denmark.

¹A. B. Chen and A. Sher, Phys. Rev. B **23**, 5360 (1981).

²K. C. Hass, H. Ehrenreich, and B. Velický, Phys. Rev. B **27**, 1088 (1983).

³J. Kudrnovský, V. Drchal, M. Šob, N. E. Christensen, and O. K. Andersen, Phys. Rev. B **40**, 10029 (1989).

⁴L. C. Davis, Phys. Rev. B **28**, 6961 (1983).

⁵J. E. Bernard and A. Zunger, Phys. Rev. B **36**, 3199 (1987); A. Zunger, S.-H. Wei, L. G. Ferreira, and J. E. Bernard, Phys. Rev. Lett. **65**, 353 (1990).

⁶H. Holloway and G. Jesion, Phys. Rev. B **26**, 5617 (1982).

⁷M. A. Tamor, L. C. Davis, and H. Holloway, Phys. Rev. Lett. **52**, 946 (1984).

⁸We refer the reader for the details concerning the TB-LMTO-CPA method to our recent papers: J. Kudrnovský, V.

Drchal, and J. Mašek, Phys. Rev. B **35**, 2487 (1987); J. Kudrnovský and V. Drchal, *ibid.* **41**, 7515 (1990).

⁹O. K. Andersen, O. Jepsen, and D. Glötzel, in *Highlights of Condensed Matter Theory*, edited by F. Bassani, F. Fumi, and M. P. Tosi (North-Holland, Amsterdam, 1985), p. 59.

¹⁰O. K. Andersen, Phys. Rev. B **12**, 3068 (1975).

¹¹S. E. Kohn, P. Y. Yu, Y. Petroff, Y. R. Shen, Y. Tsang, and M. L. Cohen, Phys. Rev. B **8**, 1477 (1973).

¹²A. Hasegawa and A. Yanase, J. Phys. C **13**, 1995 (1980).

¹³N. E. Christensen, Phys. Rev. B **30**, 5753 (1984).

¹⁴N. E. Christensen (unpublished).

¹⁵Compare, for example, the results for the Sr-rich alloy case and $\mathbf{k}=\mathbf{k}_X$. Summing up the X_3 and X'_5 contributions in Fig. 13 of Ref. 4 together, we recover the result of our Fig. 6.

¹⁶It should be noted that the Pb and Sr atoms on the cation sublattice are only the second-nearest neighbors so that the uncertainty in the choice of Pb-Sr hopping integrals is not crucial. The dominating mechanism is the strong cation-level disorder treated properly by both methods.